Atmospheric Environment 102 (2015) 260–273

Contents lists available at ScienceDirect

Atmospheric Environment

journal homepage: www.elsevier.com/locate/atmosenv

How well do satellite AOD observations represent the spatial and temporal variability of $PM_{2.5}$ concentration for the United States?

Jing Li [a, b, *], Barbara E. Carlson [a], Andrew A. Lacis [a]

[a] NASA Goddard Institute for Space Studies, New York, NY 10025, USA
[b] Department of Applied Physics and Applied Math, Columbia University, New York, NY 10025, USA

HIGHLIGHTS

- Several spectral analysis techniques were used to examine spatial and temporal variability.
- AOD and $PM_{2.5}$ variability agree well for East US but disagree for Central and West US.
- Aerosol vertical distribution is a major factor in the AOD-$PM_{2.5}$ relationship.
- Cloud-free sampling by passive sensors may also decrease AOD-$PM_{2.5}$ correlation.

ARTICLE INFO

Article history:
Received 31 July 2014
Received in revised form
25 November 2014
Accepted 1 December 2014
Available online 4 December 2014

Keywords:
PM_2
Aerosol optical depth
Satellite remote sensing
Principal component analysis
Spatial and temporal variability

ABSTRACT

Due to their extensive spatial coverage, satellite Aerosol Optical Depth (AOD) observations have been widely used to estimate and predict surface $PM_{2.5}$ concentrations. While most previous studies have focused on establishing relationships between collocated, hourly or daily AOD and $PM_{2.5}$ measurements, in this study, we instead focus on the comparison of the large-scale spatial and temporal variability between satellite AOD and $PM_{2.5}$ using monthly mean measurements. A newly developed spectral analysis technique – Combined Maximum Covariance Analysis (CMCA) is applied to Moderate Resolution Imaging Spectroradiometer (MODIS), Multi-angle Imaging Spectroradiometer (MISR), Sea-viewing Wide Field-of-view Sensor (SeaWiFS) and Ozone Monitoring Instrument (OMI) AOD datasets and Environmental Protection Agency (EPA) $PM_{2.5}$ data, in order to extract and compare the dominant modes of variability. Results indicate that AOD and $PM_{2.5}$ agree well in terms of interannual variability. An overall decrease is found in both AOD and $PM_{2.5}$ across the United States, with the strongest signal over the eastern US. With respect to seasonality, good agreement is found only for Eastern US, while for Central and Western US, AOD and $PM_{2.5}$ seasonal cycles are largely different or even reversed. These results are verified using Aerosol Robotic Network (AERONET) AOD observations and differences between satellite and AERONET are also examined. MODIS and MISR appear to have the best agreement with AERONET. In order to explain the disagreement between AOD and $PM_{2.5}$ seasonality, we further use Cloud-Aerosol Lidar with Orthogonal Polarization (CALIOP) extinction profile data to investigate the effect of two possible contributing factors, namely aerosol vertical distribution and cloud-free sampling. We find that seasonal changes in aerosol vertical distribution, due to the seasonally varying mixing height, is the primary cause for the AOD and $PM_{2.5}$ seasonal discrepancy, in particular, the low AOD but high $PM_{2.5}$ observed during the winter season for Central and Western US. In addition, cloud-free sampling by passive sensors also induces some bias in AOD seasonality, especially for the Western US, where the largest seasonal change in cloud fraction is found. The seasonal agreement between low level (below 500 m AGL), all sky CALIOP AOD and $PM_{2.5}$ is significantly better than column AOD from MODIS, MISR, SeaWiFS and OMI. In particular, the correlation between low level, all sky AOD and $PM_{2.5}$ seasonal cycles increases to above 0.7 for Central and Western US, as opposed to near zero or negative correlation for column, clear sky AOD. This result highlights the importance of accounting for the seasonally varying

* Corresponding author. Now at Scripps Institution of Oceanography, University of California San Diego, La Jolla, CA 92093, USA.
E-mail address: Jing.li@nasa.gov (J. Li).

http://dx.doi.org/10.1016/j.atmosenv.2014.12.010

aerosol profiles and cloud-free sampling bias when using column AOD measurements to infer surface $PM_{2.5}$ concentrations.

1. Introduction

Particulate matter (PM), or aerosol, is the fraction of air pollution that is most reliably associated with human disease (Anderson et al., 2012). Exposure to particles and solution droplets with diameters smaller than 2.5 μm ($PM_{2.5}$) has serious adverse effects to human health (Krewski et al., 2000; Schwartz and Neas, 2000; Pope et al., 2002). Aerosols may also have significant climate effect by altering the radiation budget, affecting atmospheric circulation and causing changes in surface temperature (Kaufman et al., 2002; Stocker et al., 2013). Therefore, particulate matter has gained increasing attention in environmental, epidemiological and climate studies. $PM_{2.5}$ is traditionally monitored by ground based sampling networks. Although the coverage of such monitoring networks is dense in several countries (Al-Saadi et al., 2005), surface measurements are still limited for many regions, making worldwide air pollution monitoring a challenging task. Satellite sensors observe aerosol optical properties from space and thus have the potential to provide surface $PM_{2.5}$ information on a global basis.

In an effort to study $PM_{2.5}$ characteristics with extensive spatial coverage, many techniques have been developed to derive $PM_{2.5}$ concentrations from satellite AOD observations, such as those from MODIS or MISR (Wang and Christopher, 2003; Liu et al., 2004; van Donkelaar et al., 2006, 2010; Gupta et al., 2006). These studies in general focused on building a relationship between AOD and $PM_{2.5}$ concentration through empirical statistical correlation (Wang and Christopher, 2003; Gupta et al., 2006; Kumar et al., 2007; Shaap et al., 2009; Kloog et al., 2011), or by taking advantage of aerosol profile information from chemical transport models (Liu et al., 2004, 2011; van Donkelaar et al., 2006, 2010; Wang et al., 2010; Kessner et al., 2013). Recently, aerosol extinction profiles observed by the CALIOP space born lidar onboard the Cloud-Aerosol Lidar and Infrared Pathfinder Satellite Observations (CALIPSO) satellite have also been used to improve the $PM_{2.5}$ – AOD relationship (Ford and Heald, 2013; Toth et al., 2013).

While promising results have been achieved in using satellite AOD for surface pollution studies, uncertainties still exist due to several factors. Aerosol vertical distribution strongly affects the column AOD – $PM_{2.5}$ relationship, since elevated aerosol layers increase the AOD but are not observed by surface measurements (Engel-Cox et al., 2006; Schafer et al., 2008; He et al., 2008). Moreover, most in-situ measurements are performed at relatively dry conditions (Collaud Coen et al., 2013) while satellites provide information under all humidity conditions, thus, aerosol property changes associated with increased relative humidity may also result in discrepancies between AOD and $PM_{2.5}$ (Shinozuka et al., 2007; van Donkelaar et al., 2010; Crumeyrolle et al., 2014). Because of this, more studies have started to integrate chemical transport models (CTMs) and satellite-measured radiances to retrieve AOD and surface PM2.5 at the same time, while taking advantages of RH effect and aerosol profile/composition in CTMs (Drury et al., 2008, 2010; Wang et al., 2010, 2012; Xu et al., 2013). On the other hand, uncertainties and limitations in satellite AOD retrievals also add to the difficulty in predicting $PM_{2.5}$. Comparison between different satellite datasets against AERONET ground truth revealed both notable bias and spread in terms of accuracy and variability (Zhang and Reid, 2006; Li et al., 2014a,b,c), due to various sources of uncertainty including calibration, cloud contamination, surface parameterization and the assumptions made in the aerosol retrieval models. Additionally, satellite retrievals are only available under cloud-free conditions, while $PM_{2.5}$ measurements can take place in the presence of clouds. Because these factors, including aerosol vertical distribution, relative humidity and cloud fraction, are spatially and temporally varying, it is thus likely that the AOD – $PM_{2.5}$ relationship also varies in space and time, which needs to be assessed specifically for different regions and seasons.

Most of the previous attempts to use AOD to derive $PM_{2.5}$ focused on hourly, or daily, collocated instantaneous measurements for individual stations or different stations combined, which does not explicitly reflect spatial and temporal variability of the parameter. Another possible issue about the analysis of coincident measurements is that random measurement noise may comprise a significant portion of the signal. However, since this is just noise, averaging the data reduces the noise level and enhances the signal portion of the measurements For example, while individual AOD measurements may agree poorly between different satellite datasets (Liu and Mishchenko, 2008), we find that the agreement is much improved when comparing monthly means (Li et al., 2013, 2014a,b,c). In addition, in observation based studies, usually only one or two satellite datasets were used to investigate AOD-$PM_{2.5}$ relationship, which could be more subject to uncertainties in individual datasets. In this study, we aim to investigate how well satellite retrieved AOD represents surface $PM_{2.5}$ variability within the continental United States, with an emphasis on spatial distribution and seasonal variability. Instead of relying on a single dataset, we use four frequently used satellite AOD datasets, namely MODIS, MISR, SeaWiFS and OMI, and ground-based measurements from AERONET. This multi-sensor approach reduces possible biases from one dataset, as the common features found in all datasets are certainly more reliable. Nonetheless, this also introduces the complication of dealing with several multi-dimensional datasets. For both efficient and effective spatio-temporal inter-comparison, we apply our newly developed Combined Maximum Covariance Analysis (CMCA, Li et al., 2014c). This technique builds upon Combined Principal Component Analysis (CPCA, Li et al., 2014b) and Maximum Covariance Analysis (MCA, Li et al., 2014a), and effectively incorporates both spatially mapped satellite data and scattered ground observations into the spectral decomposition. This analysis efficiently reduces the comparison to the first or first few dominant modes that account for the bulk of the variance in the data matrix. Moreover, since the dominant modes will maximize the covariance between satellite fields and ground observation, the coherency as well as discrepancy are readily observed by comparing the spatial modes and temporal correlation. Li et al. (2014c) demonstrated the usage of the CMCA in the comparison of spatio-temporal variability between different satellite datasets and AERONET. This paper extends its usage to AOD – $PM_{2.5}$ relationship and serves as another example of the usefulness of this technique.

In addition to the AOD observations by passive sensors, the space born lidar – CALIOP offers unique 3-D structures of the atmospheric aerosol distribution and has drawn increased attention from air quality related studies. In particular, the vertical extinction profiles provided by CALIOP allows the examination of the impact

of aerosol vertical distribution on the AOD − $PM_{2.5}$ correlation and can be used to improve $PM_{2.5}$ prediction. For example, Ford and Heald (2013) compared coincident CALIPSO vertical extinction profiles with chemical transport model, and Toth et al., 2013 compared cloud-free CALIPSO extinction profiles integrated for different levels with $PM_{2.5}$ concentration. Furthermore, CALIOP is capable of measuring aerosol extinction for both cloudy and cloud-free skies, thereby providing the opportunity to examine the effect of cloud-free sampling by the passive sensors, i.e., an investigation of the clear—sky bias introduced through the use of AOD measurements, a topic that is not covered by the previous two studies. In this paper, CALIOP Level 2 aerosol profile products are used to investigate the disagreement between satellite AOD and $PM_{2.5}$ concentration associated with both aerosol vertical distribution and cloud-free sampling.

In Section 2, we introduce the AOD, $PM_{2.5}$ and CALIOP aerosol profile datasets used in the study. Section 3 describes the spectral analysis procedure, including CMCA and MCA. The results are presented in Section 4. A summary of the results and a brief discussion are given in Section 5.

2. Datasets

2.1. Satellite AOD data

Many space born sensors have been developed to retrieval aerosol properties, with different instrumental design, viewing geometry and retrieval algorithms. Here we use four validated, frequently used, AOD datasets retrieved by MODIS, MISR, SeaWiFS and OMI, respectively. The advantage of multi-sensor approach is that the observed phenomena can be better verified using different measurements, and the strengths and weaknesses of each sensor can also be examined through the intercomparison. Li et al. (2013, 2014b, c) have detailed examples of multi-sensor data comparison.

The MODIS instrument is a multi-spectral radiometer, designed to retrieval aerosol microphysical and optical properties over land and ocean (Tanré et al., 1997; Levy et al., 2007). The 2330 km swath width of the MODIS instrument produces a global coverage in 1 or 2 days and captures most of aerosol variability due to this high sampling frequency. The MODIS on Aqua platform is used here, as Terra MODIS AOD is not as complete as Aqua over desert regions and bears calibration issues (Levy et al., 2013). The official Level 3 monthly mean AOD product at $1^\circ \times 1^\circ$ resolution is used for this study (MYD08_M3, collection 5.1, available from ftp://ladsweb.nasacom.nasa.gov/allData/51/MYD08_M3). We use QA weighted average ("*QA_Mean_Mean" variables, Hubanks et al., 2008) dark target (Levy et al., 2010) retrievals for the continental US. The MODIS AOD is interpolated to 500 nm using measurements at 470 nm and 660 nm in order to match OMI AOD reporting wavelength.

The MISR is a multi-angle sensor with nine pushbroom cameras on the EOS Terra platform. The zonal overlap of the common swath of all nine cameras is at least 360 km in order to provide multi-angle coverage in 9 days at equator, and 2 days at poles (Diner et al., 1998). Compared to MODIS, the multi-angle view of MISR performs better over bright surfaces (Kahn et al., 2005, 2010), while its lower sampling may not fully resolve short scale variability. In this study, we use version 31 Level 3 gridded monthly products, available from http://eosweb.larc.nasa.gov. The original $0.5 \times 0.5^\circ$ data resolution has been rescaled to $1 \times 1^\circ$. The rescaling is performed by assigning equal weights to each sub-grid, and the final $1^\circ \times 1^\circ$ grid is considered valid only when more than half of the sub-grids have valid data. The data are also interpolated to 500 nm using measurements at the four MISR wavelengths of 446 nm, 555 nm, 672 nm and 865 nm.

The SeaWiFS instrument was launched on the SeaStar spacecraft in 1997. It is also a wide view imager with a swath width of 1502 km and covers the global in approximately 2 days. The SeaWiFS over-land aerosol retrieval uses the deep blue algorithm developed by Hsu et al. (2004, 2006). The AOD data over land has been validated using AERONET measurements (Sayer et al., 2012). Here we use the standard Level 3 monthly mean AOD product Version 004, available from http://mirador.gsfc.nasa.gov/). The data are converted to 500 nm using the reported AOD values at 412 nm, 490 nm and 670 nm.

The OMI sensor (Levelt et al., 2006) on the EOS Aura satellite has been providing global aerosol measurements since October 2005. The OMI instrument also has a wide swath of 2600 km and produces daily global coverage. The AOD data used here are derived from the UV algorithm (OMAERUV, Torres et al., 2007). OMAERUV makes use of the instrument's two near-UV channels to retrieve AOD and single scattering albedo at 388 nm, and the 500 nm AOD reported in the standard product is converted according to the spectral dependence of the assumed aerosol model (Torres et al., 2007, 2013; Ahn et al., 2008). While the reliability of the 500 nm AOD is affected by aerosol model assumptions, comparison with AERONET, MODIS and MISR showed reasonable agreements (Torres et al., 2007; Ahn et al., 2008). Moreover, the upgraded OMI algorithm by Torres et al. (2013), which makes use of aerosol layer information derived from CALIPSO and AIRS, produces noticeable improvements in the retrieval of dust and smoke aerosols. And the evaluation work by Ahn et al. (2014) on the upgraded algorithm indicated improved agreement with ground based observation and comparable accuracy with MODIS deep blue algorithm and MISR retrieval over arid and semi-arid areas. Here we use Collection 003 data from the upgraded algorithm at $1 \times 1^\circ$ spatial resolution, available from Goddard Earth Sciences Data and Information Services Center (http://mirador.gsfc.nasa.gov/).

The period of study is chosen to be January 2005 to December 2010, which represents the longest overlapping record for all four datasets.

2.2. AERONET AOD

In order to verify the results obtained from satellite data, AERONET ground-based AOD measurements are employed as the ground truth. AERONET (Holben et al., 1998) is a ground-based sun-photometer network with over 400 stations globally. The AERONET AOD is derived from direct beam solar measurements (Holben et al., 2001) at two UV and five visible channels. The data used are the Version 2 Level 2 quality assured and cloud screened (Smirnov et al., 2000) monthly mean AOD product, available at http://aeronet.gsfc.nasa.gov/. Since AERONET is also used in the spectral analysis which requires the construction of the temporal covariance matrix, we select 52 stations in the US primarily based on the completeness of the temporal record from January 2005 to December 2010. Usually we require at least 8 monthly observations per year from 2005 to 2010. However, several stations in the Central and Western US are manually added to produce a seasonable spatial coverage. Gaps in the data are filled by linearly interpolating the de-seasonalized time series and then adding back the multi-year averaged seasonal cycle. A comparison between the interpolated and original time series suggests no obvious error caused by the interpolation (figures not shown). The AERONET AOD is converted to 500 nm using measurements from 380 nm to 870 nm by applying a 2nd order polynomial fitting of ln (AOD) vs. ln (wavelength), as recommended by Eck et al. (1999).

2.3. $PM_{2.5}$ data

The $PM_{2.5}$ concentrations are measured using the Federal Reference Method (FRM), and the data are obtained from the EPA Technology Transfer Network (TTN) Air Quality System (AQS) database (http://www.epa.gov/ttn/airs/airsaqs/). The data are 24-hr observations and we calculate monthly means for all months with more than 10 total measurements. Again, to meet the need of constructing the temporal covariance matrix, only sites with a complete record (no missing data) from 2005 to 2010 are selected. By an initial check of the distribution of the stations, we find the density of the sites much higher for Eastern US than for Central and Western US. This uneven distribution may result in biases in the spectral analysis, i.e., the variability for the Eastern US will

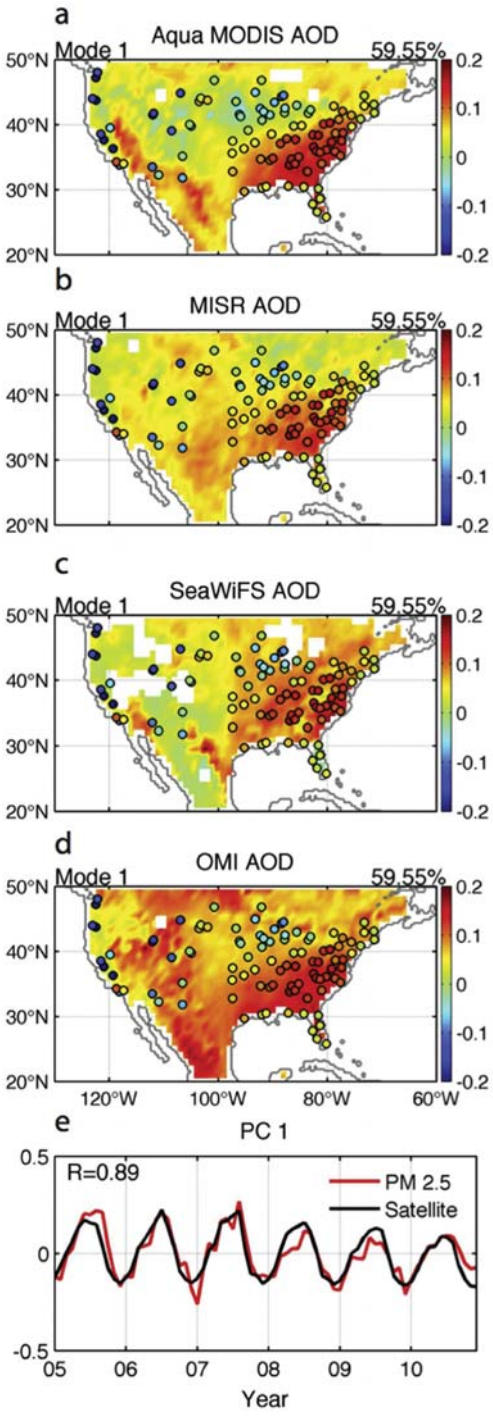

Fig. 1. The first mode of CMCA analysis between MODIS (a), MISR (b), SeaWiFS (c) and OMI (d) AOD and surface $PM_{2.5}$. This mode explains ~60% of the total variance and captures the bulk of the variability in the datasets. The number on the top right corner of panels a to d is the exact variance explained by this mode. The "*R*" value on panel e is the correlation coefficient between the two time series (PCs). Both time series exhibit distinct summer-winter seasonal cycles. The spatial maps indicate good agreement over the Eastern US but less agreement for the Central and Western US.

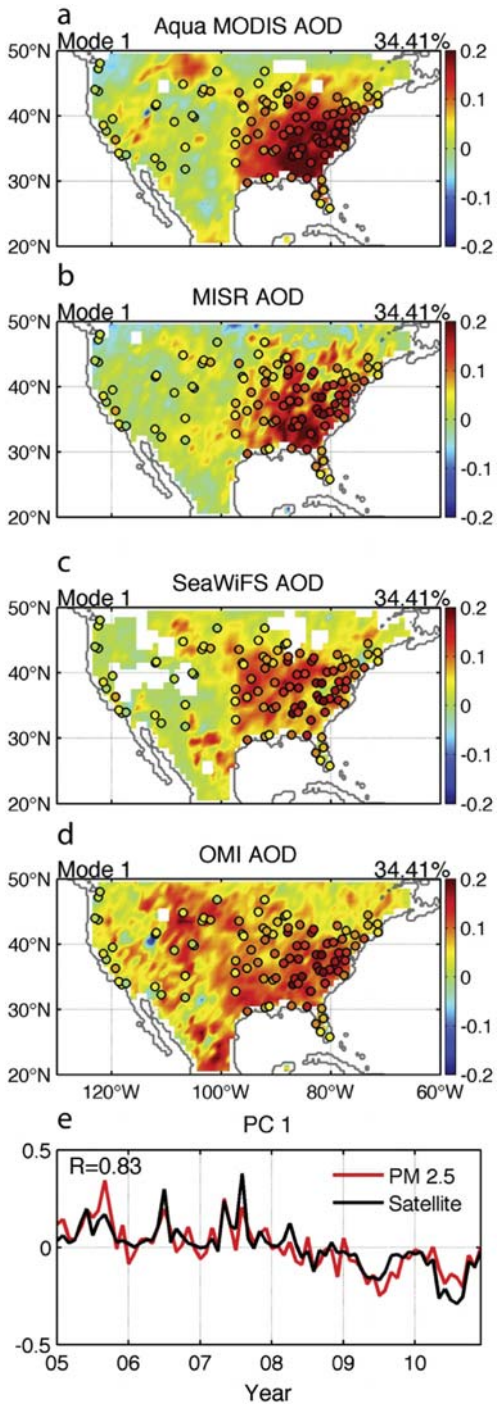

Fig. 2. Mode 1 of CMCA analysis of de-seasonalized data. The spatial patterns (a–d) agree very well. The PC time series (e) are also highly correlated, and exhibits a continuous decrease from 2007 to 2010.

outweigh that of Central and Western US. To avoid this issue, we further consolidate Eastern US sites by averaging the data and location of all sites that fall within each $1 \times 1^{\circ}$ satellite grid. The final $PM_{2.5}$ dataset consists of monthly mean data from 98 sites/grids. Their distribution can be seen from the maps in the results section, in particular, Fig. 5.

2.4. CALIOP aerosol profile product

Aerosol extinction profiles provided by the CALIOP instrument are used to gain an understanding of aerosol vertical distribution as well as all sky vs. clear sky sampling. 532 nm extinction profiles from the Version 3.01 CALIOP Level 2 5 km Aerosol Profile (L2_05kmAProf, Winker et al., 2007, 2013) for the four years from 2007 to 2010 are utilized. The data are filtered following the criteria used to create gridded Level 3 products (Winker et al., 2013). Specifically, negative extinction near the surface that are below -0.2 km^{-1}, noisy spikes (detection of 80-km aerosol layer), and isolated aerosol layer above 4 km that are adjacent to ice clouds are removed. Cloud aerosol distinction (CAD) scores and extinction quality control flags (QC) are also ensure data quality, and only layers with CAD scores between -20 and -100 and QC equals 0, 1, 16 or 18 are considered as reliable aerosol signals. In order to obtain low level AOD, we first convert the above mean sea level (AMSL) to above ground level (AGL), by extracting the mean of DEM Surface Elevation from the standard AMSL of each aerosol layer. We then integrate the extinction coefficients vertically from 0 to 500 m AGL.

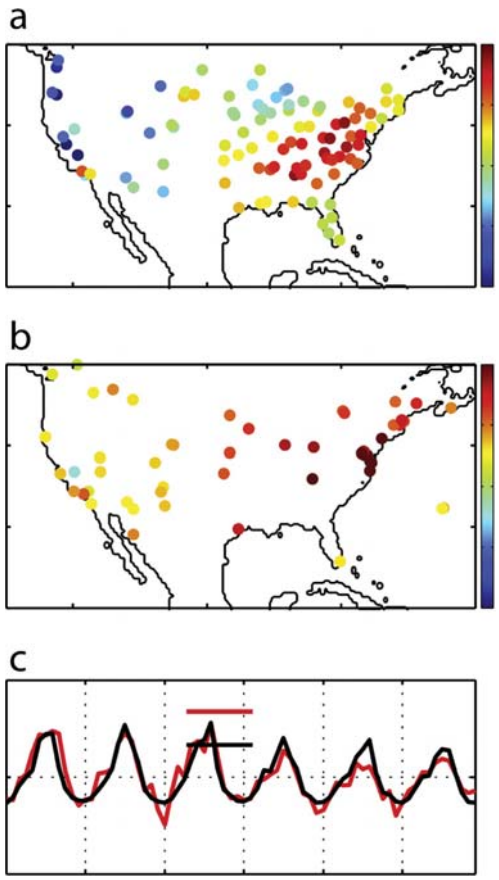

Fig. 3. The first mode of MCA analysis between $PM_{2.5}$ (a) and AERONET (b). The spatial pattern of $PM_{2.5}$ highly resembles that shown in Fig. 1. The AERONET data also exhibit similar spatial patterns to the satellite datasets shown in Fig. 1. Their PC time series (c) are also highly correlated at 0.91.

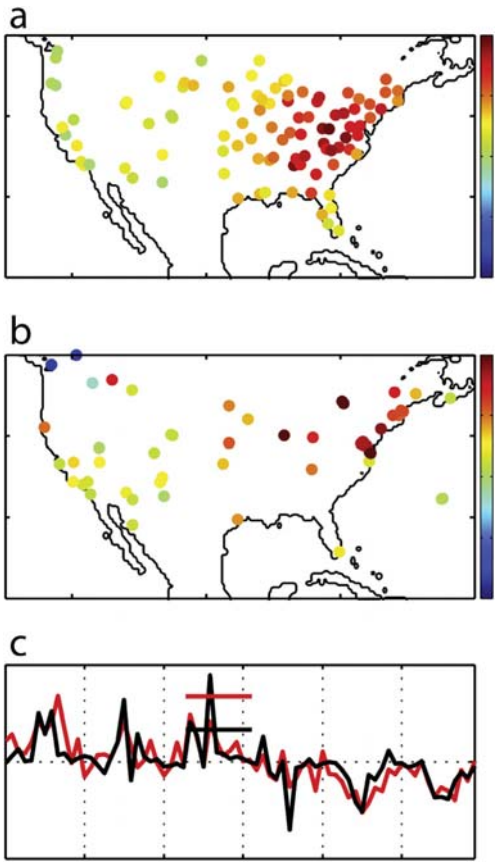

Fig. 4. The first mode of MCA analysis for the de-seasonalized $PM_{2.5}$ (a) and AERONET AOD (b). The two spatial modes and time series also highly resemble those in Fig. 2, with a high temporal correlation (c).

Before determining the use of 500 m AGL, we carried out a sensitively test using different heights from 100 m to 900 m with 200 m intervals. We found that 300 m, 500 m and 700 m results are quite similar. The 100 m level tends to be influenced by surface extinction and also has much fewer samples, while the seasonal variability for 0–900 m integrated AOD are too close to the total column. We therefore choose 500 m AGL to roughly represent low level AOD. The low level AOD fraction is then defined as the fraction of this low level AOD in the total column AOD. For cloud-free sampling, we exclude any profile that has at least one cloud layer detected, whose CAD score ranges between 20 and 100 and Vertical Feature Mask (VFM) indicates the type as cloud. A cloud fraction dataset is also generated simultaneously. Note that the cloud fraction referred to here is really the "aerosol cloud fraction", because it is used to assess the impact of cloud layers on aerosol detection. We first count the total number of profiles that contain aerosol layers, and then the number of profiles that contain both aerosol and cloud layers. The ratio of the latter to the former is then considered as cloud fraction. Calculated CALIOP total column AOD, low level AOD fraction and cloud fraction are gridded into $2.5 \times 2.5^{\circ}$ spatial resolution for better display purposes (CALIPSO sampling is sparse so finer resolution will result in holes in the spatial maps).

3. Spectral analysis methods – CMCA and MCA

Spectral decomposition methods are both effective and efficient in finding the major spatial and temporal variability in one or more high dimensional datasets. They have the advantages of not only reducing data dimension, but also allowing the simultaneous

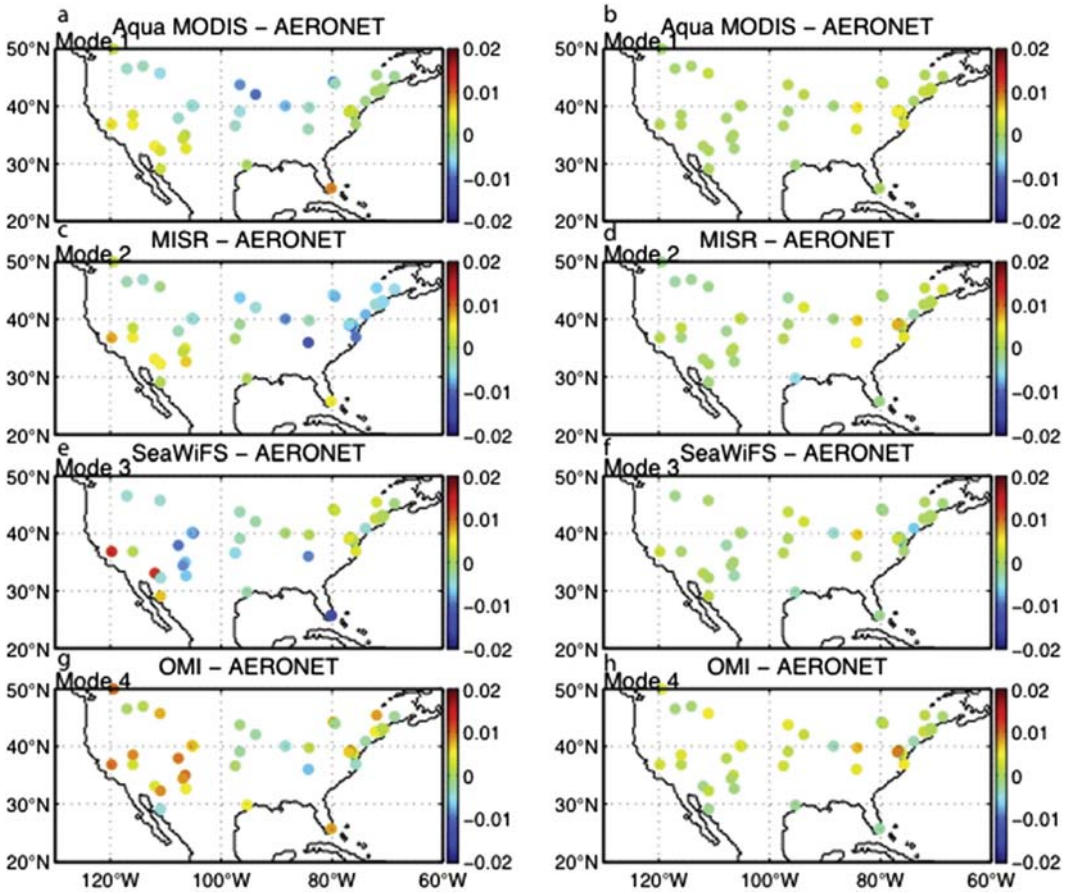

Fig. 5. Difference between satellite modes and AERONET mode for full dataset (left) and de-seasonalized dataset (right). The differences are in general larger for the full dataset than de-seasonalized dataset (as evidenced by the red and blue points), indicating good agreement on interannual variability but less agreement on seasonal variability. (For interpretation of the references to color in this figure legend, the reader is referred to the web version of this article.)

examination of both spatial and temporal variability. Here, the MCA is used to find the dominant modes between AERONET AOD and $PM_{2.5}$ datasets, while CMCA is applied to the combined satellite AOD data field and $PM_{2.5}$. The detailed mathematical description of these two methods can be found in Li et al. (2014a, 2014c), respectively, and here we only briefly describe these two methods.

MCA is also known as Singular Value Decomposition (SVD) analysis (Bretherton et al., 1992; Björnsson and Venegas, 1997). It finds the coupled modes of variability between two datasets of the same or different physical parameters, through the orthogonal decomposition of their cross covariance matrix. Each mode consists of a spatial pattern and a time series (PC) for each dataset. Similar to the traditional EOF method, this is a dimensionality reduction technique as the leading modes with largest singular values can recover most of the covariance in the two high dimensional datasets. In addition, maximizing the covariance implies that the leadings modes from the two data fields both have reasonably high correlation and respectively describes a large fraction of the variance in the two datasets. Moreover, this method is particularly suitable for scattered ground-based observations, as it has no restriction on the spatial resolution or mapping of the two data fields being decomposed.

CMCA is a novel technique based on MCA and Combined Principal Component Analysis (CPCA, Li et al., 2014b). It is developed to bridge the gap between multi-sensor satellite observations and ground observations in spectral analysis. Because MCA can only be applied to two data fields while we hope to incorporate all available satellite datasets, the multiple satellite datasets are first combined into one large data matrix as:

$$\mathbf{X_{sat}} = \begin{bmatrix} \mathbf{X_{MODIS}} \\ \mathbf{X_{MISR}} \\ \mathbf{X_{SeaWiFS}} \\ \mathbf{X_{OMI}} \end{bmatrix} \quad (1)$$

where $\mathbf{X_{sat}}$ is the combined data matrix, $\mathbf{X_{MODIS}}$, $\mathbf{X_{MISR}}$, $\mathbf{X_{SeaWiFS}}$ and $\mathbf{X_{OMI}}$ are the four satellite data matrices, respectively. Next, MCA is performed on this combined data field and surface $PM_{2.5}$ data. In this way, the major common modes of variability from different satellite datasets as well as $PM_{2.5}$ data will be extracted. Note that the combining of different datasets as Equation (1) requires equal weight of each data field. It is therefore not suitable to combine satellite with ground observations, or two different parameters such as AOD and $PM_{2.5}$. Detailed explanation of this prerequisite is given in Li et al. (2014b, c).

MCA and CMCA are performed both on full dataset with the seasonal cycle left in, in order to examine seasonal variability, and on the anomaly dataset to compare interannual variability. The anomaly dataset is constructed by removing the multi-year averaged seasonal cycle from the time series at each location, and the terms "de-seasonalized" and "anomaly" will be used interchangeably in the rest of the paper to refer to this dataset. The coherency and discrepancy between AOD and $PM_{2.5}$ datasets are reflected in the correlation of the time series, and in the agreements and disagreements between the spatial patterns of each mode.

4. Results

4.1. CMCA results for satellite AOD and $PM_{2.5}$

CMCA is first performed on the full dataset. Because aerosol variability is usually dominated by distinct seasonal cycles, the leading modes will reflect seasonal variability. Note that for full data analysis the observation at each location is still centered by removing the temporal mean.

The first mode is shown in Fig. 1. This mode accounts for ~60% of the total variance, while the variance drops to 12% for mode 2 and to below 10% for other higher order modes (figure not shown). We therefore only examine Mode 1 as the dominant component. Each CMCA mode comprises of a spatial pattern for each satellite data field as well as $PM_{2.5}$ data field, a shared time series for all satellite data fields and a time series for $PM_{2.5}$. The spatial mode for $PM_{2.5}$ is superimposed on top of the satellite spatial patterns for direct comparison. We first note that the correlation between the time series of satellite AOD (black curve in the bottom panel of Fig. 1) and that of $PM_{2.5}$ (red (in web version) curve in the same panel) are highly correlated at 0.89. This is an indication of coherent temporal variability. We then turn to the spatial patterns. The spatial distribution of the $PM_{2.5}$ signal in general exhibits three clusters: Eastern US which has strong positive signals, Central to Central Western US (East to California) showing mild negative signals, while strong negative signals are found for US West Coast. Because PC 1 is associated with a distinct summer-winter seasonal cycle, the $PM_{2.5}$ spatial distribution suggest that $PM_{2.5}$ variability over Eastern US bears the same seasonality as PC 1 with summer peaks. For Central US, the seasonality may be slightly out of phase as PC 1 or has additional peaks, which results in its weak projection on this PC and will be further examined. While for Western US, the seasonal cycle is likely opposite to that of PC 1. With respect to the satellite AOD, less spatial variability is found in all of the four spatial maps. Despite some internal differences, the four satellite datasets all indicate strong positive signals for Eastern US, which is consistent with $PM_{2.5}$. MISR and OMI also show positive signals for the rest of the continent, while MODIS and SeaWiFS have positive anomalies in the West Coast but neutral signals elsewhere. In addition, OMI appears to have a high bias throughout the study domain, which indicates that this dataset may exhibit an overall stronger seasonal variability for the entire continental US. In short, comparison between satellite AOD and $PM_{2.5}$ only reveals agreement for Eastern US. For Central and Western US, AOD and $PM_{2.5}$ show different or even opposite seasonal variability. Differences are also found among satellite AOD themselves. These issues will be examined in detail in the next few sections.

Next, we continue to examine the representation of AOD in terms of $PM_{2.5}$ interanual variability through CMCA decomposition of the de-seasonalized dataset. Similar to the full dataset, the first mode for the anomaly data is dominant, explaining ~34% of the variance, while the variance decreases to 7% for Mode 2. The spatial patterns and time series associated with Mode 1 are shown in Fig. 2. The two PCs, plotted on the bottom panel of Fig. 2, again suggest high correlation. This PC exhibits a decreasing trend, especially for the latter half of the time period from 2007 to 2010. In addition, AOD and $PM_{2.5}$ also agree on many peaks, such as those in 2006 and 2007, as well as many weaker anomalies. The agreements between the spatial patterns of AOD and $PM_{2.5}$ shown in Fig. 2 appear much better than that of the full dataset (Fig. 1). The spatial patterns (upper four panels of Fig. 2) clearly highlights the eastern part of the US where strong positive signals are observed in both AOD and $PM_{2.5}$, while no obvious projection of this PC is found for the rest of the continental US. The time evolution of this mode, shown in the lowest panel of Fig. 2, exhibits a decreasing tendency, especially from 2007 to 2010. The spatial pattern combined with the PC indicates a decrease in both column AOD and surface $PM_{2.5}$ concentration for Eastern US. Mode 1 for different satellite datasets largely agrees, with MODIS, MISR and SeaWiFS showing nearly identical spatial variability. The OMI signal is also comparable with the other three datasets for Eastern US, although it still has an overall high bias for Western US. MODIS appears to have a slightly high bias for Eastern US, which suggests a stronger temporal decrease for MODIS AOD.

4.2. MCA results for AERONET AOD and $PM_{2.5}$

In the previous section, we noted both agreements and disagreements between AOD and $PM_{2.5}$, as well as between the individual satellite datasets. Because satellite data are subject to various sources of uncertainty, it is necessary to verify the satellite data using more accurate ground-based measurements. Therefore, in this section, we present spectral decomposition analysis between AERONET AOD and $PM_{2.5}$ and compare the results with those for the satellite datasets.

Fig. 3 shows the dominant mode of MCA analysis between AERONET AOD and $PM_{2.5}$, which explains ~65% of the variance. It is clearly seen that the $PM_{2.5}$ spatial pattern are quite similar to Mode 1 of Fig. 1, with the same three clear regional clusters: strong positive signals for Eastern US, weak negative signals for Central US and strong negative signals for Western US. With respect to the AERONET spatial pattern, almost all sites indicate positive anomalies, and the signal is strongest for the Eastern US. This feature is also largely consistent with the spatial patterns of the satellite datasets shown in Fig. 1. Moreover, the PCs of AERONET AOD and $PM_{2.5}$ are also highly coherent with a 0.91 correlation.

The first mode of the de-seasonalized AERONET AOD and $PM_{2.5}$ dataset is presented in Fig. 4. This mode accounts for ~36% of the variance, which is significantly higher than that for the other high order modes. Again, it is encouraging that both the spatial patterns and time series of this mode highly resembles those for the de-seasonalized analysis between the satellite and $PM_{2.5}$ data previously shown in Fig. 2. The AERONET AOD and $PM_{2.5}$ spatial variability also agrees well, both having strong positive anomalies over the Eastern US and neutral signals over Central and Western US. The correlation between the PCs is 0.73, slightly lower than the satellite result but still significant. This might be due to some interpolation in order to fill the gaps in the AERONET time series for certain stations. Nonetheless, the agreement between Figs. 2 and 4 confirms the variability represented by the satellite datasets.

A more quantitative evaluation of the satellite modes is made by examining the difference between the satellite spatial patterns shown in Figs. 1 and 2 and those for AERONET shown in Figs. 3 and 4. The distribution of the differences is plotted in Fig. 5. The left column of Fig. 5 shows the difference between the modes for the full dataset, and the right column for the anomaly data. By quickly comparing the left and right columns of Fig. 5, we can clearly see that the difference for the anomaly modes (right column) is much lower that for the full dataset. The difference for the anomaly modes varies between −0.05 and 0.05 (note this is the amplitude of variability rather than absolute AOD value) at the majority of the stations. This result further supports that interannual variability is well represented by all four satellite datasets. While for the full dataset (left column), relatively larger differences are found. In general, MODIS and MISR agree better with AERONET than SeaWiFS and OMI. Nonetheless, MODIS appears to have lower signals for Central US. Lower signals are also found for MISR but mostly lie in Eastern US. SeaWiFS has lower variability for the Western US except for two stations in California, while OMI has an overall high bias for the western part. Because Mode 1 of the full dataset

represents seasonal variability, and significant differences also reside in the AOD and $PM_{2.5}$ modes, we consider the representation of column AOD to surface $PM_{2.5}$ is more uncertain in terms of seasonal variability than interannual variability. Accordingly, the next two sections will focus on finding the causes of the difference in the spatial modes shown in Figs. 1 and 3 and investigating possible sources of uncertainty.

4.3. Seasonal cycle investigation

The CMCA and MCA results point out differences in the seasonal variability between AOD and $PM_{2.5}$, as well as between different satellite datasets and AERONET, and suggest that these differences are mostly concentrated in the Central and Western US. However, spectral analysis itself does not explicitly reveal the exact source of the differences, i.e., whether the seasonal cycles for these regions are completely out of phase, or only have phase shifts. The major usefulness of these techniques is to efficiently identify places with more uncertainties for further examination. Recall that the spatial patterns of $PM_{2.5}$ exhibit three regional clusters with different degrees of coherency with AOD, we thus divide the data into these three groups accordingly and compare the averaged seasonal cycles between different AOD datasets and $PM_{2.5}$ concentration. The grouping maps of the $PM_{2.5}$ and AERONET stations are shown in Fig. 6. The red (in web version) sites represent the Eastern US where the best agreements are found between AOD and $PM_{2.5}$, Central US sites agree less well and are colored in green (in web version), and Western US sites where the least agreement is found are colored in blue (in web version). For the satellite data, the grid box that contains the $PM_{2.5}$ site is used to represent the data for that station.

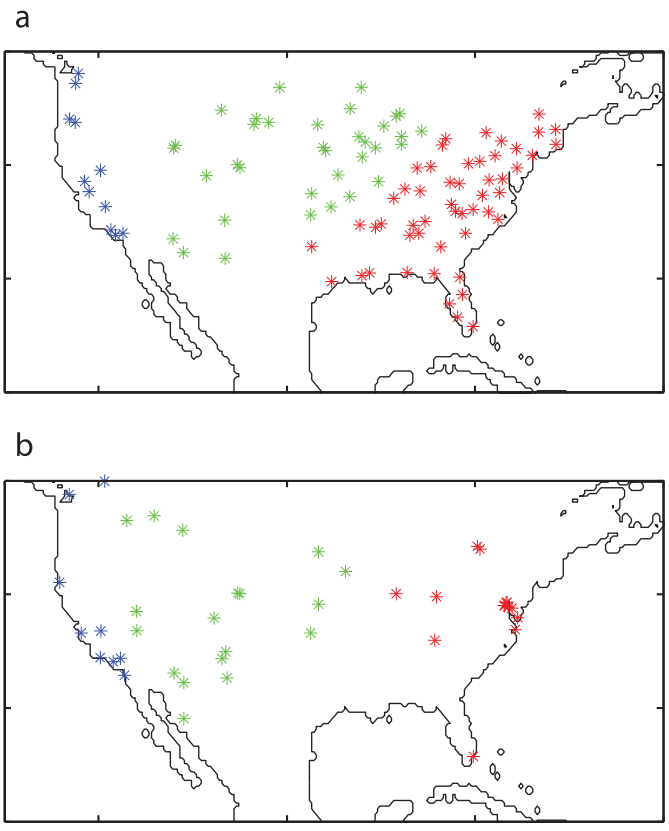

Fig. 6. Grouping of $PM_{2.5}$ (a) and AERONET (b) sites. Red: Eastern US; Green: Central US; Blue: Western US. (For interpretation of the references to color in this figure legend, the reader is referred to the web version of this article.)

The multi-year averaged seasonal cycles for the three regions: Eastern US, Central US and Western US, are shown in Fig. 7. $PM_{2.5}$ data are plotted in thick gray lines on the right axis with a different scale. In this comparison, our emphasis is on variability, which is reflected by the shapes of the seasonal cycles, rather than the absolute values.

For the Eastern US, AOD and $PM_{2.5}$ both exhibit highest values during the summer months from June to August, and lower values for the rest of the year. Satellite AODs uniformly reach a minimum in winter. However, $PM_{2.5}$ slightly increases from October to February, and the lowest values are found for early fall (September and October) and spring (March to May). This phenomenon is not seen in satellite column AOD, which suggests a possible change in the vertical distribution of aerosols in winter.

For the Central US, the AOD and $PM_{2.5}$ seasonal cycles behave more differently. While AOD still shows a single peak in the seasonal variability, $PM_{2.5}$ displays a semi-annual feature, with two peaks located in July and January, respectively. The January peak is even higher that the July one. This behavior is responsible for the weak negative projection of $PM_{2.5}$ data on the summer-winter seasonal cycle represented by PC 1, i.e., part of the $PM_{2.5}$ summer maximum is captured by this PC, however, because the winter maximum is stronger, the overall signal becomes negative. Also note that the seasonal cycles for the satellite and AERONET datasets are also not consistent and exhibit phase shifts. OMI and AERONET both have maximum AOD in July. MISR AOD does not have evident changes from April to July, while MODIS and SeaWiFS exhibit spring maxima. These differences result in the disagreements between satellite and AERONET spatial modes as shown by Fig. 5.

As expected, the Western US shows the largest discrepancy between AOD and $PM_{2.5}$. For this region, the seasonal variability for these two parameters is completely reversed. The AOD data still indicate spring-to-summer maxima, similar to Eastern and Central US, while $PM_{2.5}$ peaks in winter. This is consistent with the inference from the MCA and CMCA modes, in which Western US $PM_{2.5}$ sites appear as strong negative signals. Also the seasonal peak of the AOD for MISR, OMI and SeaWiFS slightly shifts to the spring while MODIS and AERONET suggest summer maxima.

Overall, AOD exhibits single annual cycles throughout the US. The maximum is usually found during the summer months, although some satellites have spring peaks for Central and Western US. However, the $PM_{2.5}$ seasonality is not consistent across the US continent. For the Eastern US, the $PM_{2.5}$ seasonality agrees with the AOD data in terms of summer-winter variability. Central US data exhibits a semi-annual cycle. While for the Western US, the $PM_{2.5}$ data exhibits a seasonality that is opposite to that of the AOD. The differences between the Eastern-Western US $PM_{2.5}$ seasonality has also been documented by Bell et al. (2007), who found that different species, namely sulfates and nitrates, are responsible for the East and West $PM_{2.5}$ variability, respectively. Previous studies (Engle-Cox et al., 2004, 2006; van Donkelaar et al., 2006; Paciorek et al., 2008; Toth et al., 2013) also found that the correlation between AOD and $PM_{2.5}$ is higher for Eastern US but is lower or even negative for Western US. This is suggested to be due to the more uniform vertical distribution of aerosols and relatively large signals due to widely distributed anthropogenic sources (Engel-Cox et al., 2006) in the Eastern US. In the next section, we further examine possible causes of these East-West differences between AOD and $PM_{2.5}$ seasonality using CALIOP lidar profile data.

4.4. CALIOP data analysis

The CALIOP instrument provides a unique 3-D view of the global atmosphere through active lidar observations. It is also capable of retrieving aerosol information in the presence of clouds. Therefore,

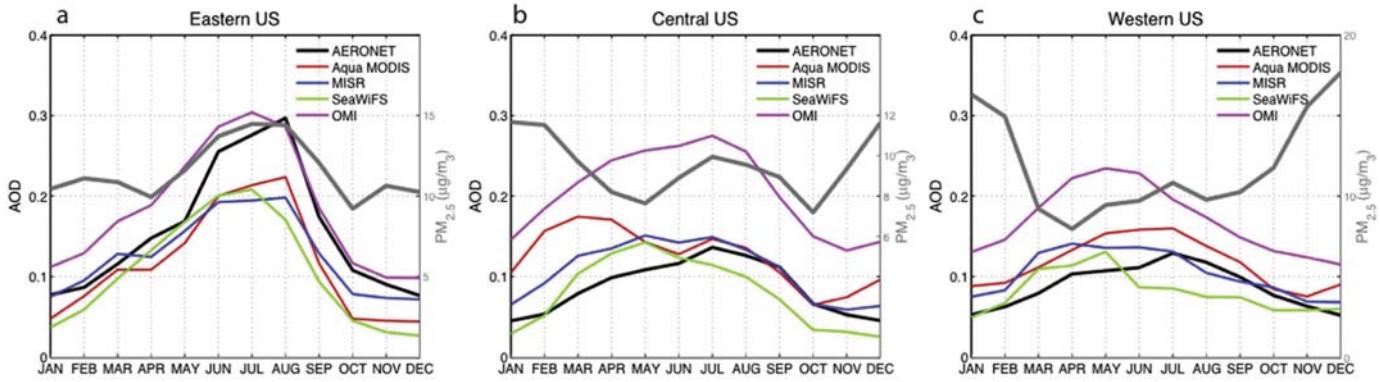

Fig. 7. Comparison between AOD and $PM_{2.5}$ multi-year averaged seasonal cycles for Eastern US (a), Central US (b) and Western US (c), the three groups shown in Fig. 6. (The $PM_{2.5}$ average cycle is shown by the heavy gray line) The seasonal cycles agree well for Eastern US. For Central US, AOD data exhibit summer-winter seasonal cycles (MODIS data peaks in the spring), while $PM_{2.5}$ shows semi-annual variability with two peaks in the winter and summer, respectively. The AOD and $PM_{2.5}$ seasonal cycles are reversed for the Western US.

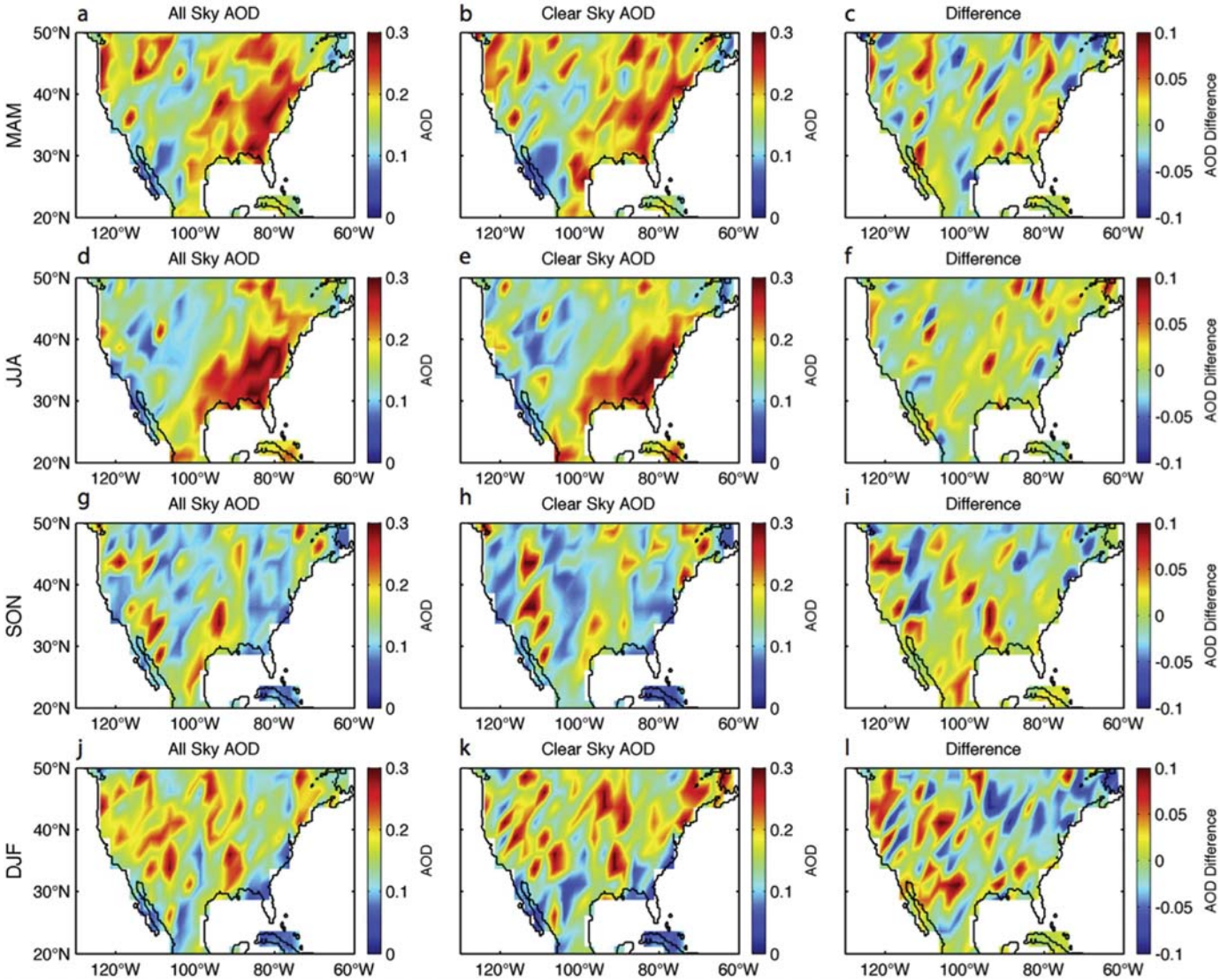

Fig. 8. All sky AOD, clear sky AOD, both integrated using CALIOP aerosol extinction profiles, and their differences for the four seasons: spring (MAM), summer (JJA), fall (SON), and winter (DJF). Cloud sampling has the most impact during the winter season and over the Central and Western US.

it allows us to examine the impact of two important factors: aerosol vertical distribution and the restriction to cloud-free sampling required for satellites, on the AOD – $PM_{2.5}$ seasonal correlation. The latter issue has not been examined before in studies of AOD-$PM_{2.5}$ correlation using CALIOP data (e.g., Ford and Heald, 2013; Toth et al., 2013). We create four datasets for the sensitivity studies: 1) all sky total column AOD; 2) clear sky total column AOD; 3) all sky AOD integrated using aerosol extinction from 0 to 500 m above surface; 4) clear sky AOD integrated using aerosol extinction from 0 to 500 m above surface. The last two datasets will be referred to as all sky low level AOD and clear sky low level AOD respectively. We then compare the seasonal cycles of these four datasets respectively with that of the $PM_{2.5}$ concentration, in order to identify the contribution of these two factors.

CALIOP all sky column AOD, clear sky column AOD and their differences (all sky minus clear sky) for the four seasons are shown in Fig. 8. The seasonal maps are multi-year averages for the 2007–2010 period used for the study. Overall, both all sky and clear sky column AOD are higher in the spring and summer and lower in the fall and winter. During the spring and summer seasons, the largest AOD signal comes from the Eastern US, while for the other two seasons, the AOD values are comparable between the Western US and Eastern US. From Fig. 8c, we see that cloud-free sampling will indeed introduce some bias with respect to total AOD. The influence appears strongest for the winter and weakest for summer. Spatially, the Western US is, in general, more prone to cloud sampling impact. From the seasonal cloud fraction maps (Fig. 9), we can see that winter and spring seasons have higher cloud fraction, especially for the western part of the continent, which is consistent with the spatial and temporal pattern of the all sky and clear sky AOD differences.

Fig. 10 shows the seasonal low AOD for all sky and clear sky conditions, as well as their differences. Comparing Figs. 8 and 10, the differences between column AOD and low level AOD are clearly seen: while total column AOD reaches maximum in the summer, low level AOD is highest during the winter. Even for the Eastern US, winter low level AOD is comparable to the summer and spring values. This is a clear indication of a seasonal change in aerosol vertical distribution, and that in winter, more aerosols will be concentrated close to the surface, which contribute to surface level aerosol loading although the total column aerosol decreases. This is likely attributed to the fact that the mixing layer (or boundary layer) is usually lower in winter than in summer (Seidel et al., 2010). The low level AOD fraction of the total column AOD is plotted in Fig. 11 for all sky conditions, which shows that in winter, low level AOD accounts for a larger fraction of total column AOD. The seasonal contrast is most pronounced for the Central US. Nonetheless, the results for the Eastern and Western US also indicate notable changes. By comparing the right most column of Figs. 8 and 10, we find that the impact of clouds on low level AOD exhibits similar patterns to that on column AOD for all seasons except DJF. During DJF, the impact of cloud-free sampling is stronger (with largest all sky/clear sky difference) on low level AOD than on column AOD, especially for Northeastern US.

Finally, we compare the Eastern, Central and Western US AOD seasonal cycles for the four datasets with that for $PM_{2.5}$ and calculate the correlations. Figs. 12 and 13 shows total column and low level AOD comparisons, respectively. All sky AODs are shown in black curves while clear sky AODs are shown in red (in web version). The "*R*" values indicate the correlation coefficients between all sky AOD and $PM_{2.5}$ (black) and clear sky AOD and $PM_{2.5}$ (red (in web version)). From Fig. 12, we find that the seasonal cycles of column AOD is positively correlated with $PM_{2.5}$ only for Eastern US. The correlation for Central and Western US is improved for all sky AOD, although still quite low compared to that for the Eastern US. However, the comparison between low level AOD and $PM_{2.5}$ indicates much better agreements for Central and Western US. The correlation further improves under all sky conditions. For Central US, the correlation between all sky low level AOD and $PM_{2.5}$ seasonal cycles is 0.78, as opposed to −0.15 for clear sky column AOD. For Western US, this value is 0.71, while that for clear sky total AOD is −0.67. For Eastern US, although the correlation for low level AOD under all sky conditions is not improved, it is important to note that the low level AOD under both clear sky and all sky conditions shows an increase in winter and spring compared to column AOD (Fig. 13), which is consistent with $PM_{2.5}$. The higher correlation for total AOD should be mostly attributed to the smoothness of the time series.

By analyzing and comparing different subsets of CALIOP data, we find that the agreement between the seasonality of AOD and $PM_{2.5}$ is much improved for all three parts of the US. The improvement is greatest for Central and Western US, the two exact regions with most disagreements between satellite/AERONET AOD

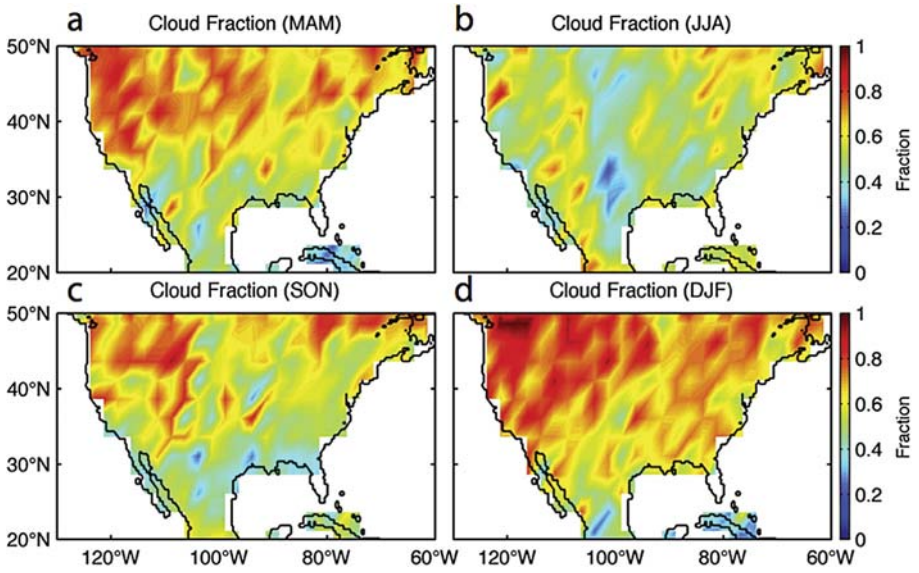

Fig. 9. CALIOP cloud fraction for the four seasons. Cloud fraction is highest for winter and spring, especially for Western US.

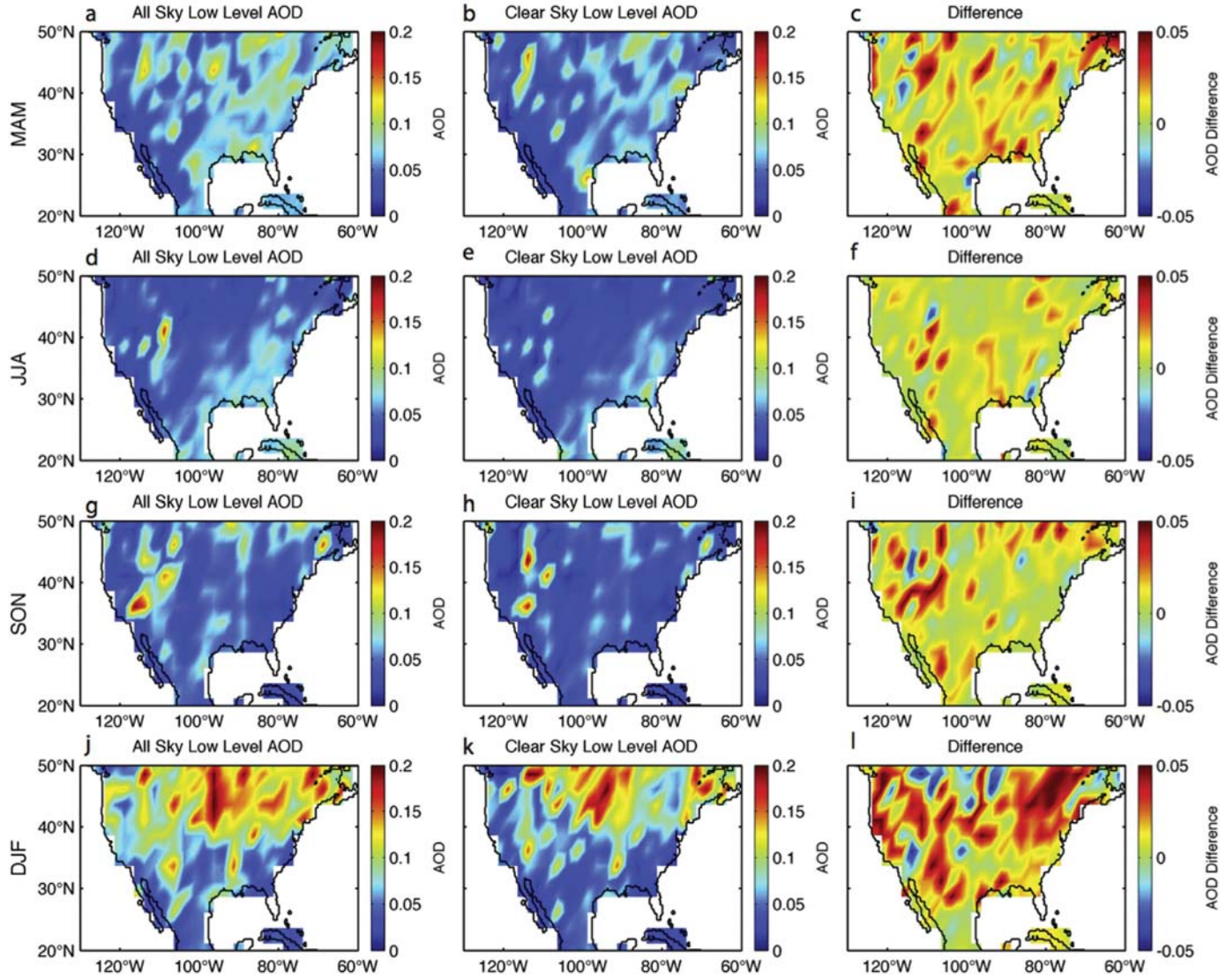

Fig. 10. Seasonal low level AOD (below 500 m) for all sky, clear sky and their differences. Different from Fig. 8, low level AOD shows higher values in winter than in the other three seasons. Cloud has similar impact on low level AOD, except for Northeastern part during the winter, where the impact of cloud-free sampling is stronger on low level AOD than total column AOD (Fig. 8).

and $PM_{2.5}$. Cloud-free sampling also introduces additional uncertainties, especially for Western US. All sky low level AOD in general provides the best representation of $PM_{2.5}$ variability.

5. Conclusions and discussions

In this paper, we investigate the representativeness of column Aerosol Optical Depth (AOD) retrieved by different satellite sensors to surface $PM_{2.5}$ concentrations for different parts in the continental United States. Comparison is focused on large-scale spatial and temporal variability, and both seasonal and interannual scales are examined. Spectral decomposition techniques, including Combined Maximum Covariance Analysis (CMCA) and Maximum Covariance Analysis (MCA), are used to isolate the dominant and correlated modes of variability from AOD and $PM_{2.5}$ datasets. Aerosol Robotic Network (AERONET) AOD is used to verify the spatial and temporal patterns of the satellite data. Aerosol extinction profile data from Cloud-Aerosol Lidar with Orthogonal Polarization (CALIOP) is further adopted to test the influence of aerosol vertical distribution and cloud-free sampling on the relationship between AOD and $PM_{2.5}$ seasonality.

While the relationship between satellite AOD and $PM_{2.5}$ is a topic of continuous interest and has been extensively investigated before, our study has several unique aspects in that (1) we are examining whether or not the space-time variability of the satellite AOD data can be used to infer the space-time variability of PM2.5 on time scales from seasonal to inter-annual using monthly mean data; (2) We are using a novel technique, Combined Maximum Covariance Analysis (CMCA), which allows us to combine multiple gridded satellite data (spatial maps at monthly time steps) with the sparser sampled AERONET and/or PM2.5 station data (also monthly averaged data) into a single combined analysis of the space-time variability eliminating the need to collocate the data in space and time. (3) We are using the CALIOP data to investigate the effect that cloud has on the AOD-PM2.5 relationship through comparisons of all-sky and clear-sky data.

There are several main findings of this study: 1) CMCA analysis shows spatially, good agreement between AOD and $PM_{2.5}$ for the

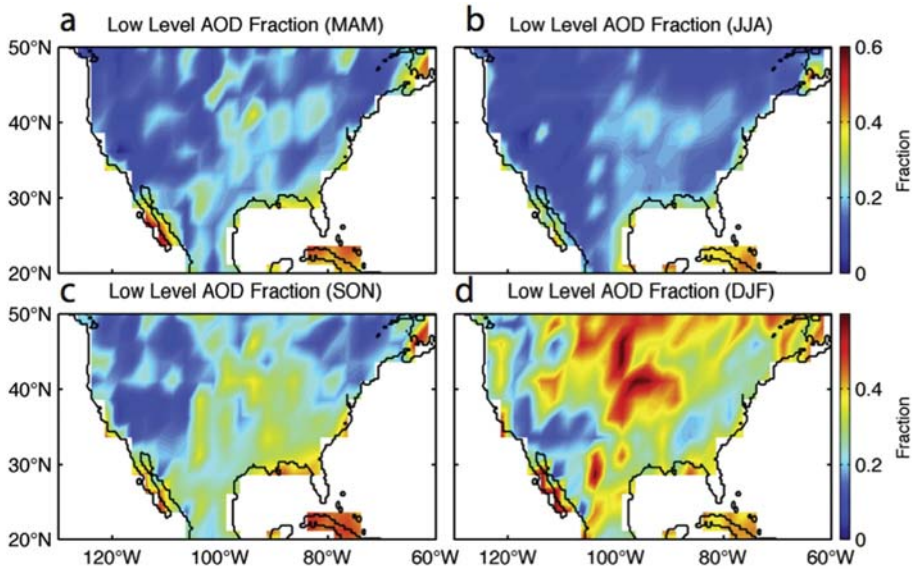

Fig. 11. Low level AOD fraction for the four seasons under all sky condition. It is clearly seen that low level AOD fraction is highest in winter throughout the US continent.

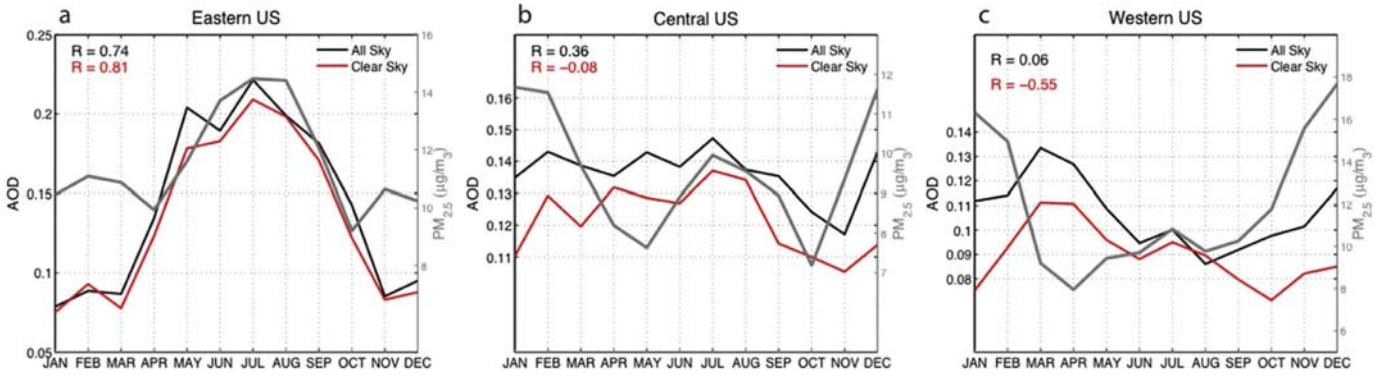

Fig. 12. Comparison between the mean seasonal cycles for CALIOP total column AOD. Black and red lines represent all sky and clear sky conditions, respectively. The *R* values on the upper left corner indicate the correlation coefficient between the corresponding CALIOP seasonal cycle and that of $PM_{2.5}$. For both Central and Western US, the correlation is improved for all sky AOD than clear sky AOD. (For interpretation of the references to colour in this figure legend, the reader is referred to the web version of this article.)

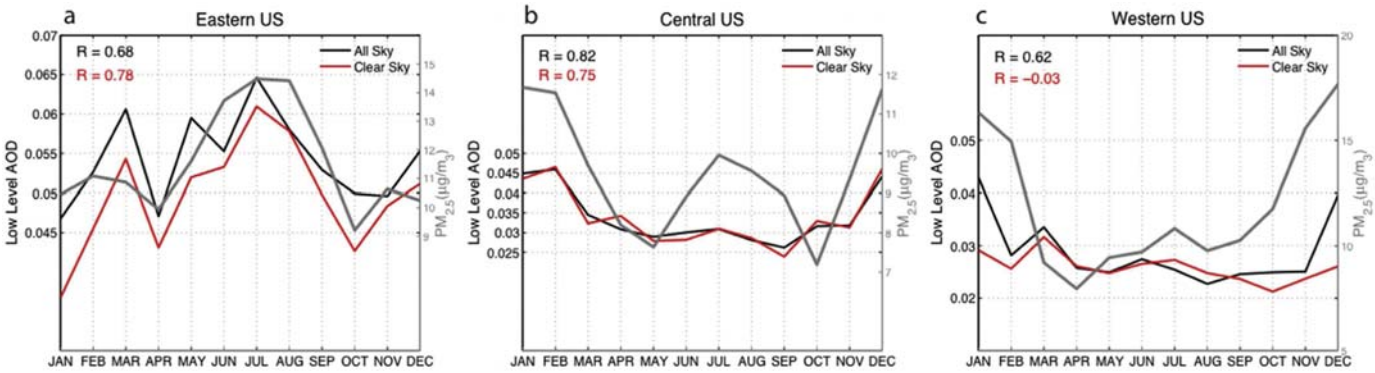

Fig. 13. The same as Fig. 12 but for low level AOD. The correlations for Central and Western US is significantly higher than total column AOD. All sky low level AOD has the best agreement with $PM_{2.5}$ for these two regions. For Eastern US, although the correlations are not improved from those in Fig. 12, the low level AOD increases in winter and early spring, which is consistent with $PM_{2.5}$ but not observed for total column AOD.

Eastern US, while major discrepancies exist for the Central and Western US; 2) Temporally, AOD and $PM_{2.5}$ agree in terms of the interannual variability, as revealed by PC 1 of de-seasonalized dataset. Most of the differences for the Central and Western US lie in the seasonal variability; 3) The spatial and temporal modes of the satellite data variability are verified using AERONET, and MODIS

and MISR appear to have better agreement with AERONET; 4) Further comparison of the AOD and $PM_{2.5}$ seasonality indicates that the AOD seasonal cycle differs from that of $PM_{2.5}$ for the Central US by missing the winter peak, while AOD and $PM_{2.5}$ show opposite seasonal cycles for the Western US; 5) further analysis suggests that the poor correlation between AOD and $PM_{2.5}$ for the Central and Western US is primarily due to aerosol vertical distribution. Cloud free sampling also contributes to the disagreement between AOD and $PM_{2.5}$, especially for the Western US. These results highlight the necessity to explicitly consider the regional and seasonal variability of aerosol vertical profile and cloud fraction when using satellite AOD to predict $PM_{2.5}$ concentrations.

Finding the relationship between AOD and $PM_{2.5}$ is essential in using satellite AOD products for surface air quality estimation and prediction. The spatial and temporal analysis presented here shows that this relationship can be highly variable for different regions and on different time scales. Therefore, localized treatment is required in building prediction models rather than a uniform statistical regression. Chemical transport models that incorporate spatially and temporally varying aerosol properties will be useful. Nonetheless, uncertainties in model parameterizations will negatively affect the accuracy of the $PM_{2.5}$ predictions. CALIOP data, as revealed here, have the potential to yield more accurate $PM_{2.5}$ predictions. However, the more limited space-time sampling of lidar instruments limits their utility. Therefore, passive sensors such as MODIS, MISR, SeaWiFS and OMI are still major data sources to infer information on particulate matter on a global basis after adjustment for aerosol vertical distribution and cloud-free sampling. The adjustment necessarily relies on information from both CALIOP and CTMs, which will be the subject of future study. In addition to the two factors considered here, several other factors, including relative humidity, coarse/dust particle fraction and aerosol diurnal cycle may also play important roles and will be investigated in future research. Moreover, the quality of satellite data is also a concern. Several problems were identified in this study, such as the overall high bias of OMI AOD variability, the seasonal cycle phase shift in MODIS data for the Central US and the high bias for the Eastern US in Aqua MODIS data, which also contribute to the disagreement between AOD and $PM_{2.5}$. Therefore, further investigation of the strength and weakness of each dataset is also required to make the best use of them for $PM_{2.5}$ applications.

Acknowledgments

The authors thank the MODIS, MISR, SeaWiFS and OMI aerosol retrieval team for providing the satellite used in this study. We also thank the AERONET team and EPA for providing the ground based AOD and $PM_{2.5}$ data. The CALIOP data is provide by the NASA Langley Atmospheric Science Data Center. This study is funded by NASA climate grant 509496.02.08.04.24. Jing Li also acknowledge Hal Maring and the NASA Radiation Science program for providing funding for this investigation.

References

Ahn, C., Torres, O., Bhartia, P.K., 2008. Comparison of ozone monitoring instrument UV aerosol products with aqua/moderate resolution imaging spectroradiometer and multiangle imaging spectroradiometer observations in 2006. J. Geophys. Res. 113 (D16).

Ahn, C., Torres, O., Jethva, H., 2014. Assessment of OMI near-UV aerosol optical depth over land. J. Geophys. Res. Atmos. 119 http://dx.doi.org/10.1002/2013JD020188.

Al-Saadi, J., et al., 2005. Improving national air quality forecasts with satellite aerosol observations. Bull. Am. Meteorol. Soc. 86 (9), 1249–1264.

Anderson, J.O., Thundiyil, J.G., Stolbach, A., 2012. Clearing the air: a review of the effects of particulate matter air pollution on human health. J. Med. Toxicol. 8 (2), 166–175.

Bell, M.L., Dominici, F., Ebisu, K., Zeger, S.L., Samet, J.M., 2007. Spatial and temporal variation in $PM_{2.5}$ chemical composition in the United States for health effects studies. Environ. health Perspect. 989–995.

Björnsson, H., Venegas, S.A., 1997. A Manual for EOF and SVD Analysis of Climate Data. CCGCR Repp. 97–101. McGill University, Montréal, QC, Canada, p. 52.

Bretherton, C.S., Smith, C., Wallace, J.M., 1992. An intercomparison of methods for finding coupled patterns in climate data. J. Clim. 5, 541–560.

Collaud Coen, M., Andrews, E., Asmi, A., Baltensperger, U., Bukowiecki, N., Day, D., Fiebig, M., Fjaeraa, A.M., Flentje, H., Hyvärinen, A., Jefferson, A., Jennings, S.G., Kouvarakis, G., Lihavainen, H., Lund Myhre, C., Malm, W.C., Mihapopoulos, N., Molenar, J.V., O'Dowd, C., Ogren, J.A., Schichtel, B.A., Sheridan, P., Virkkula, A., Weingartner, E., Weller, R., Laj, P., 2013. Aerosol decadal trends – part 1: in-situ optical measurements at GAW and IMPROVE stations. Atmos. Chem. Phys. 13, 869–894. http://dx.doi.org/10.5194/acp-13-869-2013.

Crumeyrolle, S., Chen, G., Ziemba, L., Beyersdorf, A., Thornhill, L., Winstead, E., Moore, R.H., Shook, M.A., Hudgins, C., Anderson, B.E., 2014. Factors that influence surface $PM_{2.5}$ values inferred from satellite observations: perspective gained for the US Baltimore–Washington metropolitan area during DISCOVER-AQ. Atmos. Chem. Phys. 14, 2139–2153. http://dx.doi.org/10.5194/acp-14-2139-2014.

Diner, D.J., Beckert, J.C., Reilly, T.H., Bruegge, C.J., Conel, J.E., Kahn, R., Martonchik, J.V., Ackerman, T.P., Davies, R., Gerstl, S.A.W., Gordon, H.R., Muller, J.-P., Myneni, R., Sellers, R.J., Pinty, B., Verstraete, M.M., 1998. Multiangle imaging spectroradiometer (MISR) escription and experiment overview. IEEE Trans. Geosci. Remt. Sens. 36, 1072–1087.

Drury, E., Jacob, D.J., Wang, J., Spurrs, R.J.D., Chance, K., 2008. Improved algorithm for MODIS satellite retrievals of aerosol optical depths over land. J. Geophys. Res. 113 (D16), 204. http://dx.doi.org/10.1029/2007JD009573.

Drury, E., Jacob, D.J., Spurr, R.J.D., Wang, J., Shinozuka, Y., Anderson, B.E., Clarke, A.D., Dibb, J., McNaughton, C., Weber, R., 2010. Syntehsis of satellite (MODIS), aircraft (ICARTT), and surface (IMPROVE, EPA-AQS, AERONET) aerosol observations over North America to improve MODIS aerosol retrievals and constrain surface aerosol concentration and sources. J. Geophys. Res. D14204.

Eck, T.F., Holben, B.N., Reid, J.S., Dubovik, O., Smirnov, A., O'Neill, N.T., Slutsker, I., Kinne, S., 1999. Wavelength dependence of the optical depth of biomass burning, urban and desert dust aerosols. J. Geophys. Res. 104, 31333–31350.

Engel-Cox, J.A., Holloman, C.H., Coutant, B.W., Hoff, R.M., 2004. Qualitative and quantitative evaluation of MODIS satellite sensor data for regional and urban scale air quality. Atmos. Environ. 38, 2495–2509.

Engel-Cox, J.A., Hoff, R.M., Rogers, R., Dimmick, F., Rush, A.C., Szykman, J.J., Al-SAAdi, J., Chu, D.A., Zell, E.R., 2006. Integrating lidar and satellite optical depth with ambient monitoring for 3-dimensional particulate characterization. Atmos. Environ. 40 (40), 8056–8067.

Ford, B., Heald, C.L., 2013. Aerosol loading in the Southeastern United States: reconciling surface and satellite observations. Atmos. Chem. Phys. 13, 9269–9283. http://dx.doi.org/10.5194/acp-13-9269-2013.

Gupta, P., Christopher, S.A., Wang, J., Gehrig, R., Lee, Y.C., Kumar, N., 2006. Satellite remote sensing of particulate matter and air quality assessment over global cities. Atmos. Environ. 40 (30), 5880–5892.

He, Q., Li, C., Mao, J., Lau, A.K.-H., Chu, D.A., 2008. Analysis of aerosol vertical distribution and variability in Hong Kong. J. Geophys. Res. 113 (D14), 211. http://dx.doi.org/10.1029/2008JD009778.

Holben, B.N., Eck, T.F., Slutsker, I., Tanre, D., Buis, J.P., Setzer, A., Vermote, E., Reagan, J.A., Kaufman, Y., Nakajima, T., Lavenu, F., Jankowiak, I., Smirnov, A., 1998. AERONET - a federated instrument network and data archive for aerosol characterization. Rem. Sens. Environ. 66, 1–16.

Holben, B.N., Tanre, D., Smirnov, A., Eck, T.F., Slutsker, I., Abuhassan, N., Newcomb, W.W., Schafer, J., Chatenet, B., Lavenue, F., Kaufman, Y.J., Vande Castle, J., Setzer, A., Markham, B., Clark, D., Frouin, R., Halthore, R., Karnieli, A., O'Neill, N.T., Pietras, C., Pinker, R.T., Voss, K., Zibordi, G., 2001. An emerging ground-based aerosol climatology: aerosol optical depth from AERONET. J. Geophys. Res. 106, 12067–12097.

Hsu, N.C., Tsay, S.C., King, M.D., Herman, J.R., 2004. Aerosol properties over bright reflecting source regions. IEEE Trans. Geosci. Remote Sens. 42, 557–569.

Hsu, N.C., Tsay, S.C., King, M.D., Herman, J.R., 2006. Deep blue retrievals of Asian aerosol properties during ACE-Asia. IEEE Trans. Geosci. Remote Sens. 44, 3180–3195.

Hubanks, P., King, M., Platnick, S., Pincus, R., 2008. MODIS Atmosphere L3 Gridded Product Algorithm Theoretical Basis Document Collection 005 Version 1.1. Tech. Rep. ATBD-MOD-30. NASA.

Kahn, R.A., Gaitley, B.J., Martonchik, J.V., Diner, D.J., Crean, K.A., Holben, B., 2005. Multiangle imaging spectroradiometer (MISR) global aerosol optical depth validation based on 2 years of coincident aerosol robotic network (AERONET) observations. J. Geophys. Res. 110 (D10), S04. http://dx.doi.org/10.1029/2004JD004706.

Kahn, R.A., Gaitley, B.J., Garay, M.J., Diner, D.J., Eck, T.F., Smirnov, A., Holben, B.N., 2010. Multiangle imaging spectroradiometer global aerosol product assessment by comparison with the aerosol robotic network. J. Geophys. Res. 115 (D23).

Kaufman, Y.J., Tanre, D., Boucher, O., 2002. A satellite view of aerosols in climate systems. Nature 419, 215–223.

Kessner, A., Wang, J., Levy, R., Colarco, P., 2013. Remote sensing of surface visibility from space: a look at the United States East Coast. Atmos. Environ. 81, 136–147.

Kloog, I., Koutrakis, P., Coull, B.A., Lee, H.J., Schwartz, J., 2011. Assessing temporally and spatially resolved $PM_{2.5}$ exposures for epidemiological studies using satellite aerosol optical depth measurements. Atmos. Environ. 45 (35), 6267–6275.

Krewski, D., Burnett, R.T., Goldberg, M.S., Hoover, K., Siemiatycki, J., Jerrett, M.,

Abrahamowicz, A., White, W.H., 2000. Reanalysis of the Harvard Six Cities Study and the American Cancer Society Study of Particulate Air Pollution and Mortality: a Special Report of the Institute's Particle Epidemiology Reanalysis Project. Health Effects Institute, Cambridge MA, p. 97.

Kumar, N., Chu, A., Foster, A., 2007. An empirical relationship between $PM_{2.5}$ and aerosol optical depth in Delhi metropolitan. Atmos. Environ. 41 (21), 4492–4503.

Levelt, P.F., van den Oord, G.H., Dobber, M.R., et al., 2006. The ozone monitoring instrument. geoscience and remote sensing. IEEE Trans. 44, 1093–1101.

Levy, R.C., Remer, L.A., Mattoo, S., Vermote, E.F., Kaufman, Y.J., 2007. Second-generation operational algorithm: retrieval of aerosol properties over land from inversion of moderate resolution imaging spectroradiometer spectral reflectance. J. Geophys. Res. 112 (D13), 211. http://dx.doi.org/10.1029/2006JD007811.

Levy, R.C., Remer, L.A., Kleidman, R.G., Mattoo, S., Ichoku, C., Kahn, R., Eck, T.F., 2010. Global evaluation of the collection 5 MODIS dark-target aerosol products over land. Atmos. Chem. Phys. 10, 10399–10420.

Levy, R.C., Mattoo, S., Munchak, L.A., Remer, L.A., Sayer, A.M., Hsu, N.C., 2013. The Collection 6 MODIS aerosol products over land and ocean. Atmos. Meas. Tech. Discuss. 6, 159–259. http://dx.doi.org/10.5194/amtd-6-159-2013.

Li, J., Carlson, B.E., Lacis, A.A., 2013. Application of spectral analysis techniques in the inter-comparison of aerosol data, Part I: an EOF approach to analyze the spatial-temporal variability of aerosol optical depth using multiple remote sensing data sets. J. Geophys. Res. 118, 8640–8648. http://dx.doi.org/10.1002/jgrd.50686.

Li, J., Carlson, B.E., Lacis, A.A., 2014a. Application of spectral analysis techniques in the inter-comparison of aerosol data, Part II: using maximum covariance analysis to effectively compare spatio-temporal variability of satellite and AERONET measured aerosol optical depth. J. Geophys. Res. 119, 153–166. http://dx.doi.org/10.1002/2013JD020537.

Li, J., Carlson, B.E., Lacis, A.A., 2014b. Application of spectral analysis techniques in the inter-comparison of aerosol data, part III: using combined PCA to compare spatio-temporal variability of MODIS, MISR and OMI aerosol optical depth. J. Geophys. Res. http://dx.doi.org/10.1002/2013JD020538.

Li, J., Carlson, B.E., Lacis, A.A., 2014c. Application of spectral analysis techniques to the intercomparison of aerosol data – part 4: combined maximum covariance analysis to bridge the gap between multi-sensor satellite retrievals and ground-based measurements. Atmos. Meas. Tech. Discuss. 7, 3503–3547. http://dx.doi.org/10.5194/amtd-7-3503-2014.

Liu, L., Mishchenko, M.I., 2008. Toward unified satellite climatology of aerosol properties: direct comparisons of advanced level 2 aerosol products. J. Quant. Spectrosc. Radiat. Transf. 109, 2376–2385. http://dx.doi.org/10.1016/j.jqsrt.2008.05.003.

Liu, Y., Park, R.J., Jacob, D.J., Li, Q., Kilaru, V., Sarnat, J.A., 2004. Mapping annual mean ground-level $PM_{2.5}$ concentrations using multiangle imaging spectroradiometer aerosol optical thickness over the contiguous United States. J. Geophys. Res. 109 (D22), 206. http://dx.doi.org/10.1029/2004JD005025.

Liu, Y., Wang, Z., Wang, J., Welton, E.J., Ferrare, R.A., Newson, R.K., 2011. The effect of aerosol vertical profiles on satellite-estimated surface particle sulfate concentrations. Remote Sens. Environ. 508–513.

Paciorek, C., Liu, Y., Moreno-Macias, H., Kondragunta, S., 2008. Spatio-temporal associations between GOES aerosol optical depth retrievals and ground-level PM2.5. Environ. Sci. Technol. 42, 5800–5806.

Pope III, C.A., Burnett, R.T., Thun, M.J., Calle, E.E., Krewski, D., Ito, K., Thurston, G.D., 2002. Lung cancer, cardiopulmonary mortality, and long-term exposure to fine particulate air pollution. J. Am. Med. Assoc. 287 (9), 1132–1141.

Sayer, A.M., Hsu, N.C., Bettenhausen, C., Jeong, M.-J., Holben, B.N., Zhang, J., 2012. Global and regional evaluation of over-land spectral aerosol optical depth retrievals from SeaWiFS. Atmos. Meas. Tech. 5, 1761–1778. http://dx.doi.org/10.5194/amt-5-1761-2012.

Schaap, M., Apituley, A., Timmermans, R.M.A., Koelemeijer, R.B.A., de Leeuw, G., 2009. Exploring the relation between aerosol optical depth and $PM_{2.5}$ at Cabauw, the Netherlands. Atmos. Chem. Phys. 9, 909–925. http://dx.doi.org/10.5194/acp-9-909-2009.

Schafer, K., Harbusch, A., Emeis, S., Koepke, P., Wiegner, M., 2008. Correlation of aerosol mass near the ground with aerosol optical depth during two seasons in Munich. Atmos. Environ. 42, 4036–4046.

Schwartz, J., Neas, L.M., 2000. Fine particles are more strongly associated than coarse particles with acute respiratory health effects in schoolchildren. Epidemiology 11 (1), 6–10.

Seidel, D.J., Ao, C.O., Li, K., 2010. Estimating climatological planetary boundary layer heights from radiosonde observations: comparison of methods and uncertainty analysis. J. Geophys. Res. 115 (D16), 113. http://dx.doi.org/10.1029/2009JD013680.

Shinozuka, Y., Clarke, A.D., Howell, S.G., Kapustin, V.N., McNaughton, C.S., Zhou, J., Anderson, B.E., 2007. Aircraft profiles of aerosol microphysics and optical properties over North America: aerosol optical depth and its association with $PM_{2.5}$ and water uptake. J. Geophys. Res. 112 (D12), S20. http://dx.doi.org/10.1029/2006JD007918.

Smirnov, A., Holben, B.N., Eck, T.F., Dubovik, O., Slutsker, I., 2000. Cloud screening and quality control algorithms for the AERONET database.

Stocker, T.F, et al. (Eds.), 2013. Climate Change 2013: the Physical Science Basis. Summary for Policymakers.

Tanré, D., Kaufman, Y.J., Herman, M., Mattoo, S., 1997. Remote sensing of aerosol properties over oceans using the MODIS/EOS spectral radiances. J. Geophys. Res. 102 (D14), 16971–16988. http://dx.doi.org/10.1029/96JD03437.

Torres, O., Tanskanen, A., Veihelmann, B., Ahn, C., Braak, R., Bhartia, P.K., Veefkind, P., Levelt, P., 2007. Aerosols and surface UV products from ozone monitoring instrument observations: an overview. J. Geophys. Res. 112 (D24), S47. http://dx.doi.org/10.1029/2007JD008809.

Torres, O., Ahn, C., Chen, Z., 2013. Improvements to the OMI near-UV aerosol algorithm using a-train CALIOP and AIRS observations. Atmos. Meas. Tech. 6, 3257–3270. http://dx.doi.org/10.5194/amt-6-3257-2013.

Toth, T.D., Zhang, J., Campbell, J.R., Hyer, E.J., Reid, J.S., Shi, Y., Westphal, D.L., 2013. Impact of data quality and surface-to-column representativeness on the $PM_{2.5}$/satellite AOD relationship for the Continental United States. Atmos. Chem. Phys. Discuss. 13, 31635–31671. http://dx.doi.org/10.5194/acpd-13-31635-2013.

van Donkelaar, A., Martin, R.V., Park, R.J., 2006. Estimating ground-level $PM_{2.5}$ using aerosol optical depth determined from satellite remote sensing. J. Geophys. Res. 111 (D21), 201. http://dx.doi.org/10.1029/2005JD006996.

van Donkelaar, A., Martin, R.V., Brauer, M., Kahn, R., Levy, R., Verduzco, C., Villeneuve, P.J., 2010. Global estimates of ambient fine particulate matter concentrations from satellite-based aerosol optical depth: development and application. Environ. health Perspect. 118 (6), 847.

Wang, J., Christopher, S.A., 2003. Intercomparison between satellite-derived aerosol optical thickness and $PM_{2.5}$ mass: implications for air quality studies, 2095 Geophys. Res. Lett. 30 (21). http://dx.doi.org/10.1029/2003GL018174.

Wang, J., Xu, X., Spurr, R., Wang, Y., Drury, E., 2010. Improved algorithm for MODIS satellite retrievals of aerosol optical thickness over land in dusty atmosphere: implications for air quality monitoring in China. Remote Sens. Environ. 114, 2575–2583.

Wang, J., Xu, X., Henze, K., Zeng, J., Ji, Q., Tsay, S.-C., Huang, J., 2012. Top-down estimate of dust emissions through integration of MODIS and MISR aerosol retrievals with the GEOS-Chem adjoint model. Geophys. Res. Lett. (L08), 802. http://dx.doi.org/10.1029/2012GL051136.

Winker, D.M., Hunt, W.H., McGill, M.J., 2007. Initial performance assessment of CALIOP. Geo Phys. Res. Lett. 34 (L19), 803. http://dx.doi.org/10.1029/2007GL030135.

Winker, D.M., Tackett, J.L., Getzewich, B.J., Liu, Z., Vaughan, M.A., Rogers, R.R., 2013. The global 3-D distribution of tropospheric aerosols as characterized by CALIOP. Atmos. Chem. Phys. 13, 3345–3361. http://dx.doi.org/10.5194/acp-13-3345-2013.

Xu, X., Wang, J., Henze, D., Qu, W., Kopacz, M., 2013. Constraints on aerosol sources using GEOS-Chem adjoint and MODIS radiances, and evaluation with multisensor (OMI, MISR) data. J. Geophys. Res. Atmos. 118, 6396–6413. http://dx.doi.org/10.1002/jgrd.50515.

Zhang, J., Reid, J.S., 2006. MODIS aerosol product analysis for data assimilation: assessment of over-ocean level 2aerosol optical thickness retrievals. J. Geophys. Res. 111 (D22), 207. http://dx.doi.org/10.1029/2005JD006898.